Small-hole waveguides in silicon photonic crystal slabs: efficiently utilizing the complete photonic band gap

Christian Bayer and Martin Straub*

Business Unit Spatial Light Modulators, Fraunhofer Institute for Photonic Microsystems, Maria-Reiche-Str. 2, D-01109 Dresden, Germany

[*]Corresponding author: martin.straub@ipms.fraunhofer.de

We investigate photonic crystal waveguides which are formed by holes of reduced diameter within a hexagonal lattice of cylindrical air columns in thin silicon slabs. The waveguides operate in both an even symmetry band gap and a partial gap of odd symmetry modes which under the light line form a complete two-dimensional band gap. The operating frequency is tuned by the small-hole diameter to fit in the range of both band gaps and to match a free space wavelength of 1550 nm. Their narrow bandwidth and low group velocity of light propagation renders the waveguides useful as filters or sensing elements. Due to the strong dependence of the waveguide mode characteristics on structural changes highest-precision lithographic fabrication techniques must be applied.

OCIS codes: 230.5298, 230.740, 160.5293

Introduction

Two-dimensional photonic crystal slabs are of high technological importance as they can be fabricated using well-established semiconductor processing techniques. In particular, they can be integrated monolithically into silicon or gallium arsenide microstructures. As a result, waveguides in such photonic crystal slabs have been investigated extensively [1-6]. While light is confined in the slab vertically by index-guiding, the in-plane confinement of light due to photonic band gaps allows for narrow waveguides with sharp bends [7-9], thereby facilitating integrated structures with a small footprint. For two-dimensional photonic crystals of infinite height the hexagonal lattice of air columns in a dielectric with high permittivity is favoured for its large transverse electrical (TE) polarization gap. In the two-dimensional case, at ratios of hole radius r and lattice constant a in the range of 0.4 to 0.5 overlap between the TE- and transverse magnetic (TM) polarization gaps results in a complete photonic band gap. However, photonic crystal slabs feature increasing gap frequencies when the slab is thinned down. As a result, the odd-symmetry mode gap (which corresponds to the TM polarization gap of the infinitely tall structure) is shifted beyond the light line rendering it useless for waveguide applications [3]. Therefore, we concentrate on lower bands in lattices with r/a ratio slightly lower than for the ideal two-dimensional structures with complete band gap. In these slabs the odd-symmetry gap turns into a partial gap, which is located outside the light cone. However, as even- and odd-symmetry mode gaps overlap everywhere under the light line, competing resonant modes exist only within the light cone. Therefore, the partial odd-symmetry gap can be used to aid guiding even-symmetry (TE-like) modes such as specific waveguide modes of interest, while scattering into odd-symmetry modes at discontinuities is reduced.

In this article we analyze the optical properties of hexagonal hole-lattice silicon photonic crystal slabs featuring complete band gaps outside the light cone by calculating their dispersion diagrams across the irreducible Brillouin zone. Small-hole waveguides are also characterized by their dispersion relations as determined by finite difference time domain (FDTD) simulations [10], and mode parameters such as bandwidth and group velocity are derived. The dependence of mode propagation on structural changes is studied, and ways to fabricate the photonic crystal structures are discussed.

Finite difference time domain calculations

The FDTD calculations were performed using commercial software (FDTD Solutions, Lumerical Solutions Inc. [11]). The FDTD method accounts for losses caused by light travelling apart from the slab as it happens for resonant modes inside the light cone [3]. An infinite periodic structure can be simulated by a simple cell and appropriate Bloch boundary conditions (BBC) as shown in figure 1. The structure is discretized in 26 Yee cells per lattice constant. On top and bottom of the model we use perfectly matched layers (PML) to absorb any outgoing waves [12]. Photonic crystal and waveguide modes are excited by dipoles with appropriate polarization. These sources emit short pulses covering a spectral range of 0 to 0.7 c/a. Since the simulation domain is rectangular and covers more than one unit cell of the hexagonal lattice, dipoles have to be placed in each unit cell in the same way. The relative phase of dipoles in different unit cells is set according to the BBC. By setting the BBC we follow the Γ-M-K-Γ path in the irreducible Brillouin zone [1] and analyse the system's response in order to extract resonant frequencies. Therefore, we record the time signal of the magnetic or electric field in the slab's symmetry plane and perform a Fourier transform thereof. Dispersion diagrams are obtained from calculations for both even- and odd-symmetry modes choosing fourteen wave vector values per Γ-M-K-Γ path segment.

Photonic band structures

Figure 2 shows the band structures for a slab of thickness h/a = 0.5 and hole radius r/a = 0.41. Within the light cone some of the modes are highly lossy and, hence, could not be identified, as seen in the figure from their incomplete bands. The odd-symmetry bands reveal a gap below the light line between the 2^{nd} and 3^{rd} band. As competing slab modes exist within the light cone in the same frequency range, we refer to it as a partial gap. It overlaps with the large even-symmetry gap and can aid guiding an even-symmetry waveguide mode by means of reduced scattering losses. Since the partial odd-symmetry gap is located quite close to the upper edge of the even-symmetry gap, waveguide modes also must have a comparatively high frequency. To pull even-symmetry modes down from the air band into both gaps, one row of holes is slightly reduced in diameter. This forms a photonic crystal waveguide of which mode dispersion curves are calculated in the same way as for the undisturbed the lattice. Since the Brillouin zone of a linear waveguide is one-dimensional, only reciprocal lattice vectors between Γ and K' (π/a, 0) must be accounted for [3]. Figure 3 shows two waveguide modes within the considered band gap, of which only the mode at lower frequency is investigated in detail. Its profile (figure 4, lower panel) does not show any lateral nodes, whereas the second waveguide mode at higher frequency reveals a more complex profile having a central lateral node (upper panel). Figure 3 also includes all of the slab modes of figure 2 plotted against their wave vector component in Γ-K' direction. If a waveguide mode and a slab mode share both frequency and the same wave vector component in Γ-K' direction, coupling might occur and the waveguide mode becomes lossy. Slab modes matching these conditions exist within the light cone. However, importantly, they do not appear below the light line where the waveguide modes are intended to operate.

Small-hole waveguide for 1550 nm wavelength operation

First of all, the photonic lattice must exhibit both gaps near the desired free space wavelength of 1550 nm, which corresponds to a frequency of 193.4 THz. At a slab thickness h = 350 nm a lattice constant a = 700 nm and a hole radius r = 290 nm meet this requirement. A small-hole radius r_s = 254 nm adjusts lower-frequency waveguide mode to the target wavelength. From the simulation of a single cell of the waveguide one can also extract its bandwidth, range of group velocities as well as of losses per unit cell. We define the bandwidth as the frequency range, in which the waveguide mode is below the light line, as for wave vector components at frequencies above the light line it is attenuated due to competing resonant modes. Since the waveguide mode is located close to the light cone, its bandwidth is quite small and equals only 1.4 nm. The useful bandwidth can be further limited by effects occurring in the immediate vicinity of the light line. At wave vectors close to the light line the evanescent tail of the waveguide mode may extend considerably into air and, hence, may interact with some underlying substrate. For example, a free-standing silicon membrane made from the device silicon layer of a silicon-on-insulator (SOI) wafer may incur losses due to the nearby substrate. From the dispersion relation the group velocity of the waveguide mode is obtained. For our design it ranges from 0 to 0.013 c_0, where c_0 is the velocity of light in vacuum. Thus, the small-hole waveguide excels by its slow light propagation which can be exploited, for example, in sensor applications, as the interaction time with any media is increased by two orders of magnitude. From the group velocity and the attenuation constant of the time signal in the unit cell simulation the loss per unit cell is determined. Figure 5 shows the result for the small-hole waveguide in an SOI structure with 2 µm of removed buried oxide. For most of the wave vectors between the light line and K' losses are very low (approx. 0.008 dB/a). However, close to and beyond the light line losses are strongly rising as mode confinement is reduced gradually. In the immediate vicinity of K' higher losses per unit cell are observed as the group velocity approaches zero.

Fabrication issues

In order to choose the optimum fabrication technique the spatial resolution as well as the precision and reproducibility of structural details have to be taken into account. Regarding the spatial resolution required, standard 365 nm photolithography and etching on SOI wafers may be used to fabricate the small-hole waveguide, as a minimum hole radius r_{min} = 150 nm can be achieved. However, due to the small hole edge spacing of s = 120 nm, which is required for the hexagonal hole lattice under consideration, holes must be widened afterwards by appropriate post-processing steps. After a lattice has been produced at a smaller hole radius (e.g. r = 250 nm, r_s = 214 nm), holes are extended in size to the desired radii (r = 290 nm, r_s = 254 nm) by thermal oxidation followed by etching of the oxide in a hydrofluoric acid solution. Hence, narrow silicon bars between the holes of merely s = 120 nm can be produced. Figure 6 shows an electron microscope image of an array of holes at lattice constant a = 810 nm, which was produced using a Nikon NSR-series I-line stepper. Widening the holes twice reduced the hole-to-hole spacing s from 170 nm down to less than 50 nm, thereby increasing the hole radius from 320 nm to 380 nm. A drawback of this method is the anisotropy of the oxidation of silicon, which is characterized by a slightly higher oxidation rate in the <110> direction than in the <100> direction [13]. As seen in fig. 6, holes become slightly square-shaped and, therefore, reduce the high symmetry of the hexagonal lattice. As a result, a directional dependence of the waveguide's operating frequency is introduced. Due to the narrow bandwidth, the implementation of waveguide bends requires precise adaptation of the small-hole radius to match the waveguide frequency in both directions. By contrast, using higher-resolution techniques such as 247 nm- or 193 nm-photolithography photonic crystal structures may be fabricated without sophisticated after-treatment.

To evaluate the requirements regarding structural precision and reproducibility we analyzed the dependence of the waveguide mode on minor structural changes. To pull down waveguide modes from the air band into the band gap, the radius of the waveguide holes was decreased by merely 12%. Thus, a strong dependence of the waveguide characteristics on deviations from the design is expected. Also due to its narrow bandwidth of 1.4 nm long- and short-range structural variations may strongly influence the waveguide performance. Therefore, we carried out simulations at different small-hole diameters and compared the mode frequencies at K'. The sensitivity S of the mode wavelength is defined as the change in wavelength λ upon change in the hole radius r. For the small-hole waveguide under scrutiny a sensitivity was $S = d\lambda/dr \approx 5$ was determined. Hence, it is essential to keep statistical deviations of the structural parameters extremely low. Regarding systematic deviations, a change in the hole radius of 9 nm results in a shift of the waveguide mode at $\lambda = 1550$ nm out of the complete band gap into the surrounding even-symmetry gap region.

From these considerations it appears that sub-nanometer precision of structural details is required for the waveguide to operate at 1550 nm. Thus, highest-resolution fabrication techniques such as electron beam lithography or other scanning microscopy approaches such as direct writing of structures into photoresist using scanning optical near-field microscopy must be used for fabrication of the desired structures. Photolithographic techniques, if any, may be used for applications in the mid infrared spectral range such as gas-, fluid- or biosensing exploiting specific absorption bands, or for application at even longer wavelengths.

Conclusions

We designed a photonic crystal waveguide for 1550 nm wavelength operation incorporating small holes as a line defect in thin hexagonal hole-lattice silicon photonic crystal slabs. It hosts two even-symmetry modes of different lateral symmetry in both an even-symmetry (TE-like) and a partial odd-symmetry (TM-like) band gap which combine to form a complete two-dimensional band gap below the light line. The lower-freqency waveguide mode exhibits a simple mode profile, narrow bandwidth and low group velocity, which is useful for sensing applications or filters for optical telecommunication devices. Since photonic crystals are scalable, nearly any desired operation frequency can be matched. Our analysis of the dependence of the mode characteristics on statistical and systematic deviations from the design geometry demonstrates that the waveguides have to be fabricated at highest structural precision using most advanced nanofabrication techniques.

Acknowledgements

We are grateful to J. Schmidt for coordinating the oxidation experiments and to W. Pufe for recording scanning electron microscopy images. This research was funded by the Fraunhofer Society of Applied Science within the Challenge program.

References

1. J. D. Joannopoulos et al., *Photonic Crystals-Molding the Flow of Light* (Princeton University Press, Princeton, New Jersey 08540, 2008)
2. K. Busch etal., *Photonic Crystals* (WILEY-VCH Verlag GmbH & Co.KGaA, Weinheim, 2004)
3. S. G. Johnson et al., "Linear waveguides in photonic crystal slabs", Phys. Rev. B **62**, 8212-8222 (2000)
4. M. Loncar et al., "Design and fabrication of silicon photonic crystal optical waveguides", J. Lightwave Technol. **18**, 1402-1411 (2000)
5. M. Notomi et al., "Extremely large group-velocity dispersion of line-defect waveguides in photonic crystal slabs", Phys. Rev. Lett. **87**, 253902 (2001)
6. C. Jamois et al., "Silicon-based two-dimensional photonic crystal waveguides", Photonics Nanostruct. Fundam. Appl. **1**, 1-13 (2003)
7. A. Mekis et al., "High transmission through sharp bends in photonic crystal waveguides", Phys. Rev. Lett. **77**, 3787-3790 (1996)
8. A. Chutinan and S. Noda, "Waveguides and waveguide bends in two-dimensional photonic crystal slabs", Phys. Rev. B **62**, 4488-4492 (2000)
9. S.Assefa et al., "Transmission of slow light through photonic crystal waveguide bends", Opt. Lett. 31, 745-747 (2006)
10. A. Taflove and S. C. Hagness, *Computational Electrodynamics* (Artech House Inc., Norwood, MA 02062, 2005)
11. Lumerical Solutions Inc., *FDTD Solutions*

12. J. P. Berenger, “Three-dimensional perfectly matched layer for the absorption of electromagnetic waves”, J. Comput Phys. **127**, 363-379 (1996)
13. D. B. Kao et al., “Two-dimensional thermal oxidation of silicon – I. Experiments”, IEEE Trans. Electron Devices **34**, 1008-1017 (1987)

Figure captions

1. Simulation setup for the calculation of (a) lattice and (d) waveguide bands using the FDTD method. For the lattice a rectangular cell is used instead of the primitive lattice unit cell. Small circles indicate dipole positions for excitation (d). At sides Bloch boundary conditions are set according to the outer path of the irreducible Brillouin zone (b). At top and bottom PML boundary conditions are applied. The waveguide unit cell consists of the small hole centred within an adequate number of lattice holes. The arrow indicates the direction of light propagation (e).
2. Dispersion diagram of lattice modes. The even-symmetry gap is indicated by horizontal dotted lines. Within this gap a partial odd-symmetry gap exists below the light-line marked by dashed lines. The desired operation wavelength of 1550 nm corresponds to a normalized frequency of 0.4516 and lies within both gaps.
3. Dispersion diagram of even-symmetry waveguide modes. The graph also shows slab modes already presented in figure 2 projected onto the Γ-K'-direction.
4. H_z amplitude profile of the first (bottom) and second even-symmetry waveguide mode (top) calculated at the K' symmetry point. Dark and bright areas indicate amplitude maxima as well as the phase difference of π of the magnetic field. The serrated hole edges emerge from spatial discretization within the FDTD algorithm.
5. Result of the waveguide unit cell simulation. The graph shows calculated frequency points between Γ and K' of the first TE waveguide mode and a polynomial fit thereof. Group velocity and loss per unit cell are determined by the fitted frequency data.

6. Example of hexagonal lattice of holes in silicon fabricated by 365 nm photolithography after thermal oxidation and HF-dip etching. The hole diameter is about 700 nm and silicon bars are less than 50 nm wide.

Figures

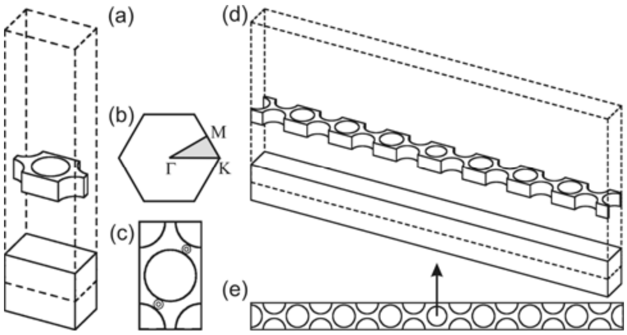

Fig. 1.

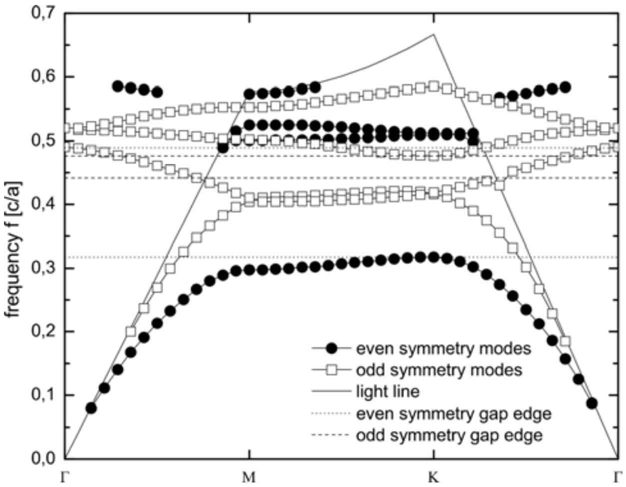

Fig. 2.

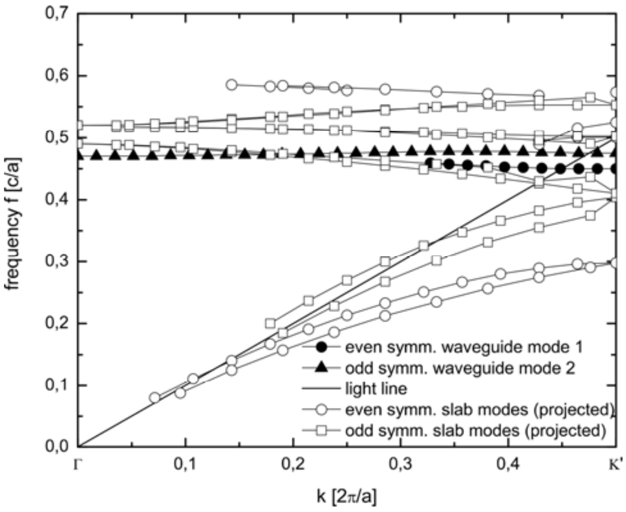

Fig. 3.

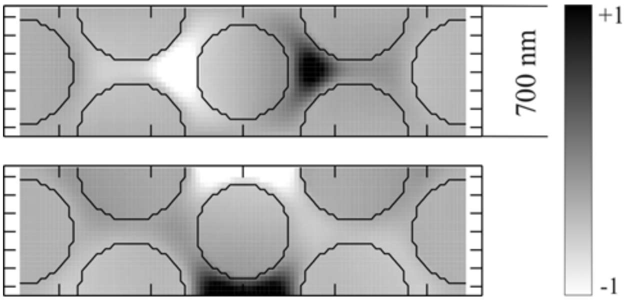

Fig. 4.

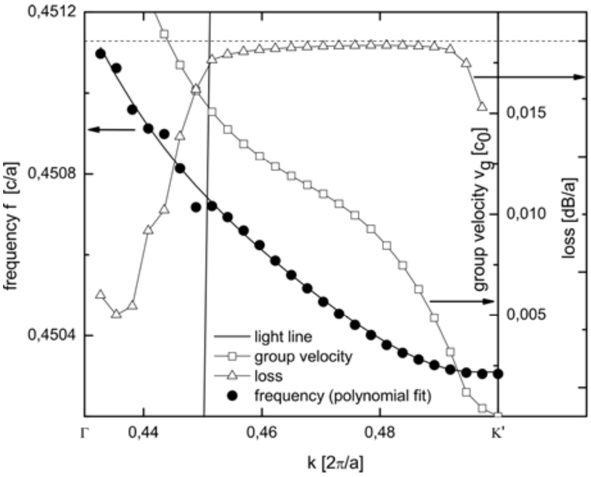

Fig. 5.

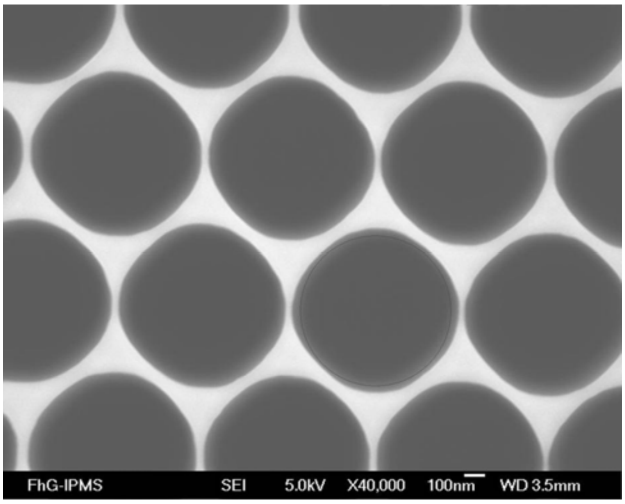

Fig. 6.